



# BENIGN NEOPLASMS OF THE UTERUS: MR IMAGING OF LEIOMYOMAS WITH RADIOLOGIC-PATHOLOGIC CORRELATION

P.V. FOTI<sup>1</sup>, C. TILOCCA<sup>1</sup>, A. SIGONA<sup>1</sup>, S. PALMUCCI<sup>1</sup>, R. FARINA<sup>1</sup>, R. CALTABIANO<sup>2</sup>,  
S. SPADOLA<sup>2</sup>, G. ZARBO<sup>3</sup>, R. ZARBO<sup>3</sup>, P. MILONE<sup>1</sup>, G.C. ETTORE<sup>1</sup>

<sup>1</sup>Radiodiagnostic and Radiotherapy Unit, University Hospital "Policlinico-Vittorio Emanuele", Catania, Italy

<sup>2</sup>Dipartimento G.F. Ingrassia – Istituto di Anatomia Patologica, University of Catania, Catania, Italy

<sup>3</sup>Dipartimento di Chirurgia Generale e Specialità Medico-Chirurgiche – Istituto di Patologia Ostetrica e Ginecologica, University of Catania, Catania, Italy

**ABSTRACT: Background:** *Leiomyomas represent the most common benign uterine tumors. Typically asymptomatic, they may determine menometrorrhagia, abdominal pain and infertility. They may be singular or multiple and may have variable size. When leiomyomas increase in size, their vascular supply may become insufficient determining different types of degeneration: hyaline, myxoid, cystic and hemorrhagic (red). Differential diagnosis includes adenomyosis, solid adnexal masses, focal contraction of myometrium and leiomyosarcomas of the uterus. Our purpose is to describe MR imaging findings, histological features and clinical aspects of uterine leiomyomas.*

**Materials and Methods:** *Our MR protocol includes sagittal, oblique coronal, oblique axial T2-weighted fast spin-echo and T1-weighted 3D gradient echo LAVA fat-suppressed sequences before and after contrast administration, and axial DWI SE EPI sequence.*

**Results:** *Non-degenerated uterine leiomyomas typically appear as well defined masses, homogeneously hypointense in comparison to the surrounding myometrium on T2-weighted images and with intermediate signal intensity on T1-weighted images. Hypercellular leiomyomas show signal intensity higher than that of non degenerated leiomyomas on T2 weighted images and present contrast enhancement after administration of mdc. Degenerated leiomyomas present variable signal intensity on T2-weighted images and on T1-weighted images obtained before and after contrast administration. Differential diagnosis with leiomyosarcoma, characterized by hemorrhagic areas, necrosis and, frequently, irregular margins may be difficult and sometimes only possible with histopathology.*

**Conclusions:** *MRI is the most accurate radiological tool in detection and localization of uterine leiomyomas. Leiomyomas characterization, often possible with MR imaging, require knowledge of pathological features and imaging findings associated with the different kinds of degeneration. MRI is an irreplaceable tool in planning the correct therapeutic strategy and in follow up after therapy.*

**KEY WORDS:** *Magnetic resonance imaging, Leiomyomas, Uterine leiomyomas, Uterine neoplasms.*

## INTRODUCTION

Leiomyomas represent the most common gynecologic tumors and are observed in 20-30% of women in reproductive age<sup>1</sup>.

Magnetic resonance (MR) is the most accurate imaging tool to identify and localize leiomyomas<sup>1,2</sup>. At MR imaging leiomyomas can show a typical signal (hypointensity on T2-weighted images); however, especially in larger tumors, may

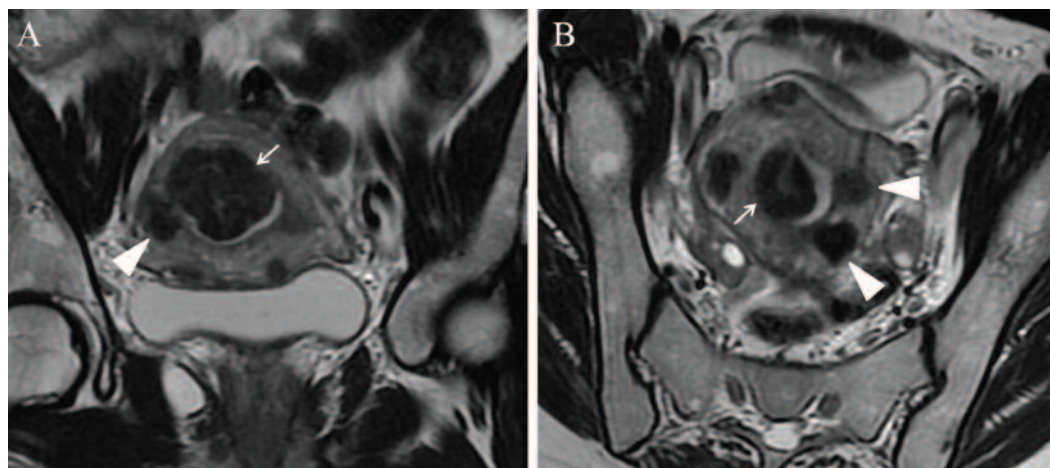


**Figure 1.** Submucosal and intramural leiomyomas in a 39 year-old woman. Oblique axial (A) and oblique coronal (B) FSE T2-weighted images reveal multiple leiomyomas without degeneration homogeneously hypointense compared to the surrounding myometrium, with submucosal (white arrows) and intramural (white arrowheads) localization.

manifest different patterns of degeneration that make their appearance widely variable. Knowledge of histological features of degenerated leiomyomas may help the radiologist to recognize and sometimes to characterize these lesions<sup>1,3</sup>.

Differential diagnosis at MR imaging include adenomyosis, solid adnexal masses, focal myometrial contractions and uterine leiomyosarcomas<sup>1,4</sup>.

In this article, we show MR imaging findings, histological features and clinical aspects of uterine leiomyomas through the description of some radiological cases analyzed in our department, many of which has been histologically confirmed. Differential diagnosis as well as our MRI protocol are exposed.

## CLASSIFICATION

Leiomyomas generally interest the myometrium of uterine corpus but they may also be found in the cervix (about 8% of cases). According to their location they are classified as submucosal (Figure 1), intramural (Figure 1) or subserosal (Figure 2). This classification has real clinical importance as symptoms and treatment options vary in relation to the different type of leiomyomas<sup>1</sup>.

Submucosal leiomyomas are the least common (about 5% of cases), but they determine clinical symptoms more frequently than the other types and can be associated with dysmenorrhea, menorrhagia and infertility<sup>5</sup>. Pedunculated submucosal leiomyomas may protrude in the cervix canal or in vagina.

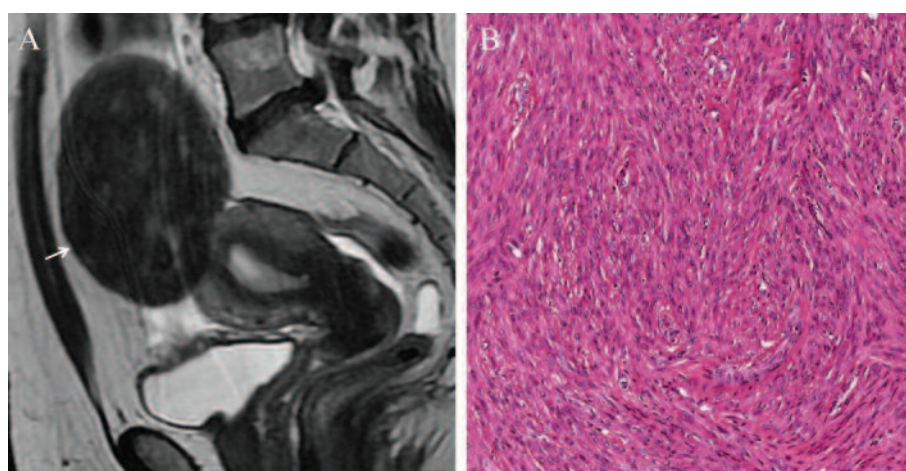


**Figure 2.** Subserosal leiomyoma in a 32 year-old woman. (A) Sagittal FSE T2-weighted image reveals a non degenerated leiomyoma homogeneously hypointense compared to the surrounding myometrium, with subserosal localization (white arrow) in the uterine fundus. (B) Histological examination (H&E 20x). Proliferation of smooth muscle cells combined in collated fibers.

Intramural are the most common leiomyomas and are often asymptomatic. They can be associated with menorrhagia or infertility, in case of compression of fallopian tubes<sup>6</sup>.

Subserosal leiomyomas may be pedunculated and may undergo torsion with clinical acute abdominal pain; they may also develop in the context of broad uterine ligament simulating an adnexal mass<sup>1</sup>.

## CLINICAL SYMPTOMS

The percentage of symptomatic patients affected by uterine leiomyomas is between 20 and 50%<sup>7</sup>. Main symptoms correlated with the presence of leiomyomas that can represent indication for surgical treatment are: bleeding, compression of adjacent organs, pain and infertility<sup>1</sup>.

### *Bleeding*

Bleeding is the most common symptom of leiomyomas; it may manifest as menorrhagia or metrorrhagia and may determine anemia. Haemorrhage can be associated with the presence of submucosal leiomyomas which determine erosion of overlying endometrium, or with intramural myomas which interfere with the normal contractile activity of myometrium determining menstrual irregularities<sup>1</sup>.

### *Compression of adjacent organs*

Voluminous leiomyomas may determine compression of adjacent anatomical structures with onset of different clinical symptoms in relation to the anatomical compartment involved. When leiomyomas develop into the anterior compartment of the pelvis may determine compression of the bladder with consequent pollakiuria or incontinence; if they growth up in the posterior compartment may compress the sigma-rectum and determine constipation. Leiomyomas developing into the broad ligament of the uterus may determine compression of the ureter with hydroureteronephrosis<sup>7</sup>.

### *Pain*

Painful symptoms may verify in about 30% of women affected by uterine leiomyomas<sup>6</sup> and may occur in case of torsion of pedunculated subserosal lesions or in case of prolapse of pedunculated submucosal lesions<sup>1</sup>. Pain may also be associated

with acute hemorrhagic degeneration that occurs more frequently during pregnancy<sup>1</sup>.

### *Infertility*

Infertility associated with uterine leiomyomas can be determined by impairment of fallopian tubes or distortion of the endometrial cavity<sup>7</sup>.

## MR IMAGING FINDINGS AND CORRELATION WITH HISTOPATHOLOGY

Magnetic resonance represents the most accurate radiological technique in identifying and localize uterine leiomyomas<sup>2</sup>. Concerning the identification of leiomyomas MRI is more sensitive than ultrasonography which has a very limited field of view<sup>8,9</sup>.

Owing to its excellent contrast resolution and multiplanar capability MRI allows to recognize the zonal anatomy of the uterus and to correctly classify the lesions as submucosal, intramural and subserosal<sup>1</sup>.

Non degenerated uterine leiomyomas have a typical appearance at MRI and appear as well defined masses, homogeneously hypointense in comparison to the surrounding myometrium on T2-weighted images (Figures 1, 2) and with intermediate signal intensity on T1-weighted images<sup>1,3</sup>. Histopathological examination reveals that non degenerated leiomyomas are characterized by a proliferation of smooth muscle cells, organised in bundles separated by a variable quantity of well vascularised connective tissue (Figure 2). Within the stroma may be present lymphocytes and numerous mast cells.

From a histological point of view hypercellular leiomyomas are characterized by an increased cellularity, but they do not present coagulative necrosis or cellular atypia. At MR imaging they show signal intensity higher than that of non degenerated leiomyomas on T2 weighted images (Figure 3 a-c) and present contrast enhancement after administration of m.d.c. On diffusion weighted imaging (DWI) may be observed areas of restricted diffusion, which are expression of the hypercellularity of the lesion (Figure 3 d-e).

When leiomyomas increase in size, their vascular supply may become insufficient determining many types of degeneration: hyaline, myxoid, cystic and hemorrhagic degeneration<sup>1,3</sup>. The type of degeneration pattern depends on how quickly the vascular insufficiency establishes<sup>4</sup> and inside

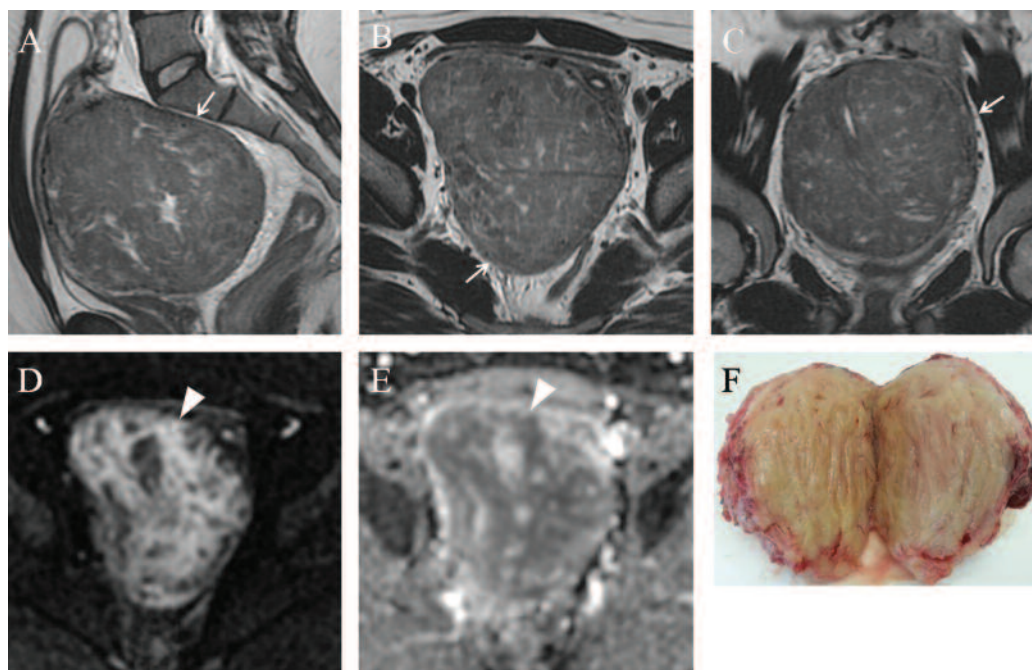


**Figure 3.** Hypercellular leiomyoma in a 28 year-old woman. Sagittal (A), oblique axial (B) and oblique coronal (C) FSE T2-weighted images reveal a voluminous leiomyoma inhomogeneously hyperintense (white arrow). (D) Axial diffusion-weighted (DW) image ( $b = 800 \text{ s/mm}^2$ ) reveals the presence of hyperintense areas into the lesion (white arrowhead), which appear hypointense (white arrowhead) in the corresponding ADC map (E) demonstrating lesion's hypercellularity. (F) Photograph of the cut surface of the resected lesion shows good MR imaging-histopathologic correlation of the leiomyoma.

the same leiomyoma different types of degeneration may coexist. Degenerated leiomyomas present variable signal intensity on T2-weighted images and on T1-weighted images obtained before and after contrast administration.

*Hyaline degeneration* is the most common type of degeneration, it occurs in more than 60% of leiomyomas and may be focal or diffuse<sup>3</sup>. At histologic examination it is characterized by deposits of collagen fibers into areas of the leiomyoma with insufficient vascular supply. At MR imaging their radiological appearance is quite similar to that of standard leiomyomas with low signal intensity on T2-weighted images (Figures 4, 6)<sup>1,3</sup>.

*Cystic degeneration* may be observed in about 4% of leiomyomas and is characterized by the presence of cystic areas of variable width<sup>3</sup>. At MR imaging the cystic components appear as roundish and well defined areas, with water-like signal intensity: low signal on T1-weighted images and high signal on T2-weighted images, without contrast enhancement (Figure 4)<sup>1,3</sup>. In some cases the cystic alteration can interest the whole extension of the leiomyoma (Figure 5).

At histologic examination *myxoid degeneration* is characterized by the backlog of glycosaminoglycans in regions with insufficient vascular supply. At MR imaging leiomyomas with myxoid degeneration show high signal intensity

on T2-weighted images and poor contrast enhancement (Figure 6)<sup>1,3</sup>.

*Red degeneration* is due the obstruction of drainage veins located at the periphery of the lesion with consequent hemorrhagic stroke and coagulative necrosis<sup>3</sup>. This condition occurs more often during pregnancy or in association with the administration of oral contraceptives and may determine systemic symptoms like abdominal pain, fever and leukocytosis<sup>1,3</sup>. At MR imaging leiomyomas with hemorrhagic degeneration may display the following pattern: diffuse or peripheral high signal intensity on T1-weighted images due to the paramagnetic effect (T1 shortening) of methemoglobin, variable signal intensity with or without hypointense peripheral ring on T2-weighted images (Figure 7). After contrast administration the lesion doesn't show enhancement due to the complete interruption of vascular supply<sup>1,3</sup>.

About 30% of leiomyomas may show a peripheral ring of high signal intensity on T2-weighted images that represents a pseudocapsule made of dilated lymphatic vessels, ectatic veins or edema and matches with the peritumoral enhancement observed on T1-weighted images after contrast administration<sup>10,11</sup>.

Other histological features observed in leiomyomas are represented by: edema, hemorrhage, necrosis and calcifications.

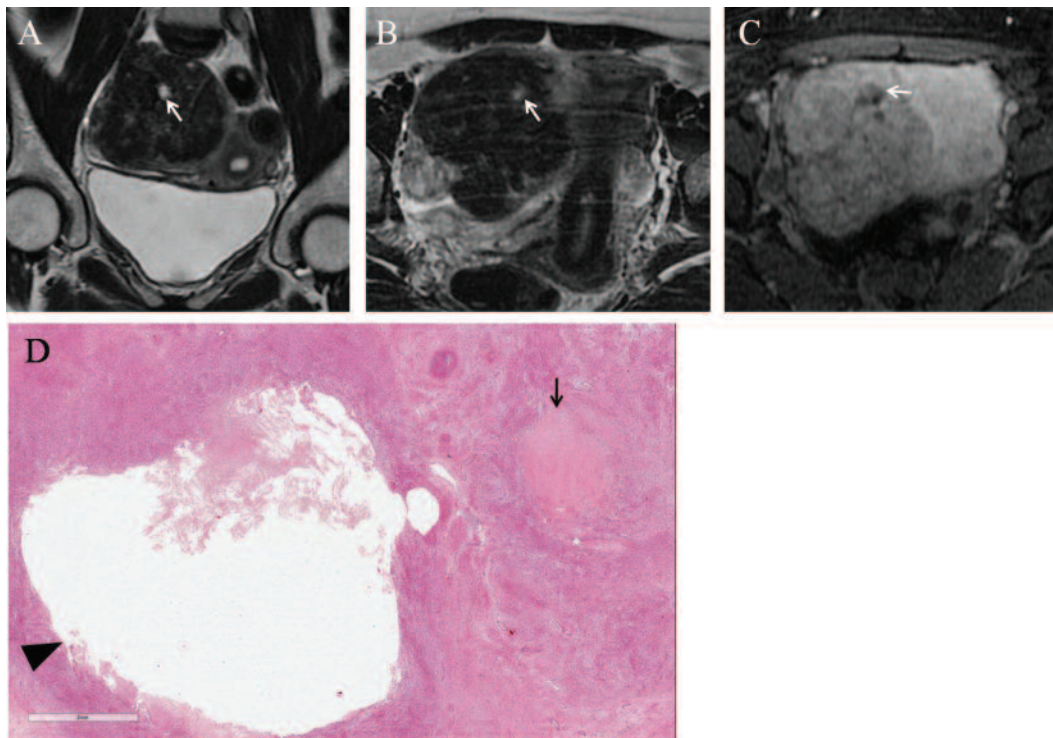


**Figure 4.** Subserosal leiomyoma with hyaline and cystic degeneration in a 42 year-old woman. Oblique axial (A) and oblique coronal (B) FSE T2-weighted images; (C) axial T1-weighted 3D gradient echo LAVA fat-suppressed image after contrast administration. Into the right broad ligament can be observed a voluminous subserosal leiomyoma which presents hypointense signal on T2-weighted images (A, B), within areas with fluid content (white arrows in A and B) which do not present contrast enhancement (white arrow in C). (D) Histological examination (H&E 1x). Focal hyaline degeneration (black arrow) and area of cystic degeneration (black arrowhead) in the context of the leiomyomatous proliferation.

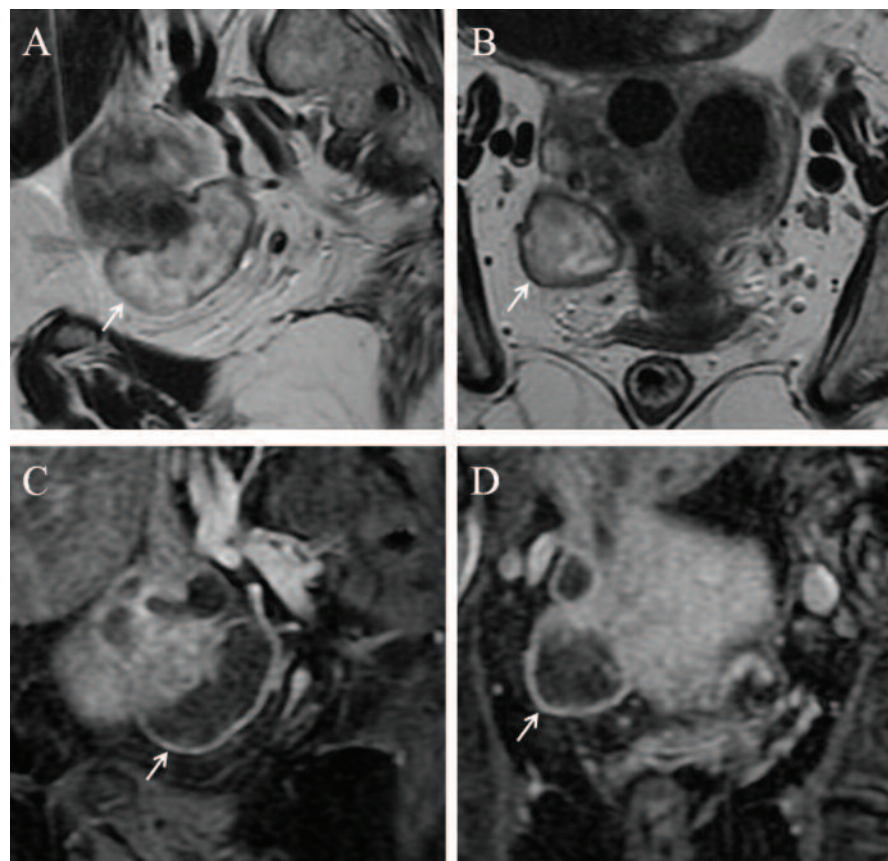


**Figure 5.** Subserosal leiomyoma with cystic degeneration in a 68 year-old woman. Sagittal (A) and oblique coronal (B) FSE T2-weighted images; sagittal (C) and oblique coronal (D) T1-weighted 3D gradient echo LAVA fat-suppressed image after administration of contrast agent. In the right side of the uterus can be observed a leiomyoma with fluid-like signal intensity, diffusely hyperintense on T2-weighted images (white arrows in A and B) and hypointense on T1-weighted images, without contrast enhancement (white arrows in C and D). Radiological findings suggest cystic degeneration.

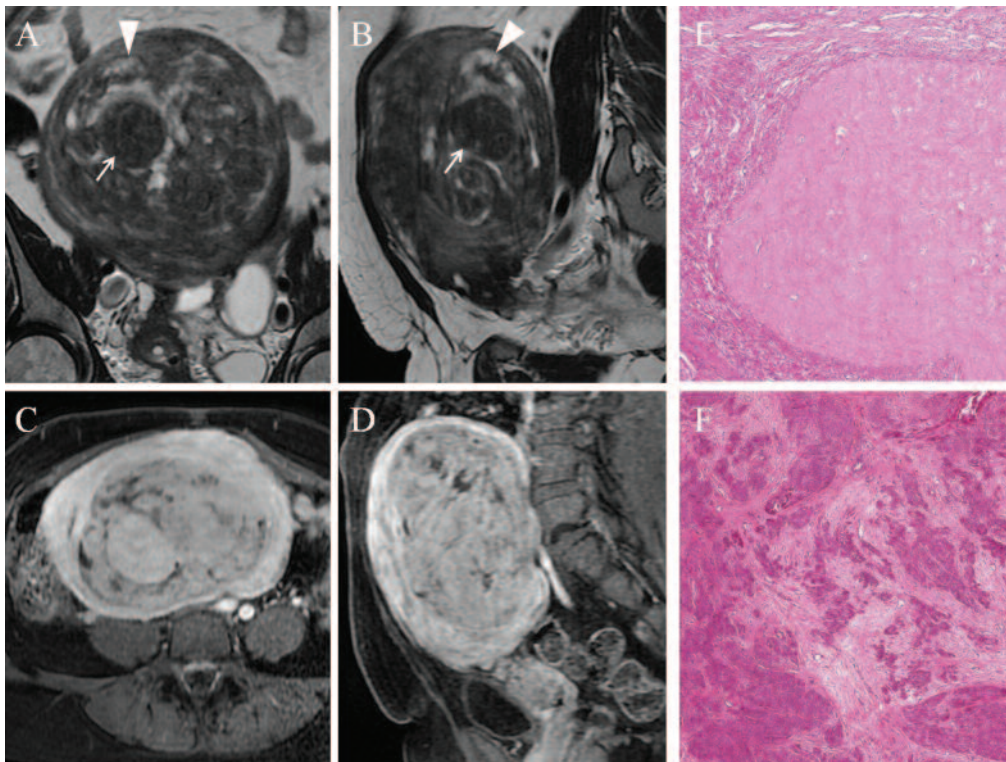


**Figure 6.** Leiomyoma with hyaline and myxoid degeneration in a 48 year-old woman. Oblique coronal (A) and sagittal (B) FSE T2-weighted images reveal a voluminous intramural leiomyoma. The mass appears inhomogeneous because of the presence of hypointense areas (hyaline degeneration) (white arrows) and hyperintense areas (myxoid degeneration) (white arrowheads). On axial (C) and sagittal (D) T1-weighted 3D gradient echo LAVA fat-suppressed images after contrast agent administration, the lesion has slightly inhomogeneous contrast enhancement. (E) Histological examination. Area of hyaline degeneration, characterized by collagen fibres deposition, surrounding by bundles of smooth muscle cells (H&E 5x). (F) Histological examination. Area of myxoid degeneration (H&E 5x).

*Edema* is a histological feature observed in about 50% of leiomyomas and it is not always correlated with degeneration<sup>3</sup>. Edema may be diffuse to the whole lesion with mottled appearance, but more frequently it prevails at the periphery of

the lesion (Figure 8)<sup>11</sup>. Leiomyomas with extensive edema, show high signal intensity on T2-weighted images due to the backlog of fluid and intense enhancement due to the retention of contrast into the abundant interstitial space<sup>3</sup>.

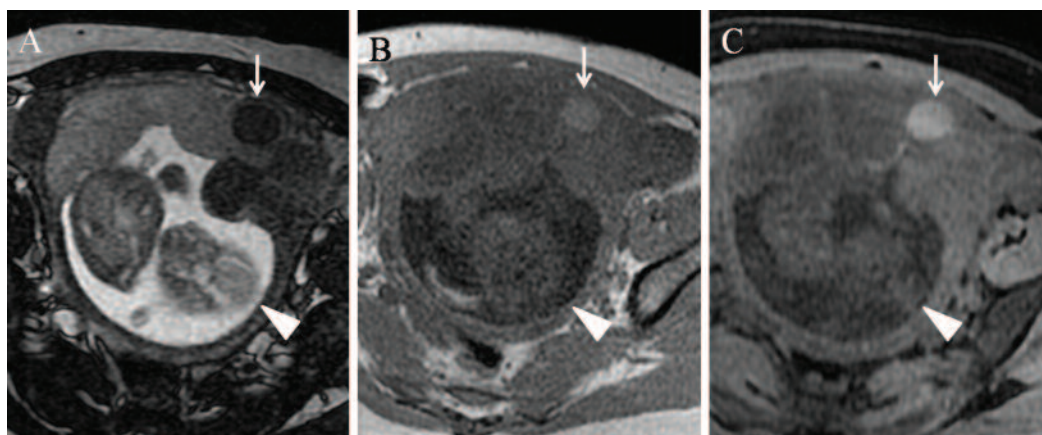


**Figure 7.** Leiomyoma with hemorrhagic degeneration in a 38 year-old pregnant woman (24<sup>th</sup> week of pregnancy). (A) Axial FSE T2-weighted image; (B) axial T1-weighted 2D gradient echo image (C) axial T1-weighted 3D gradient echo LAVA fat-suppressed image. On the left anterior side of the uterus can be seen a roundish leiomyoma (white arrows) with hypointense signal on T2-weighted image (A), hyperintense signal on T1-weighted image (B) and hyperintense signal on T1-weighted fat-suppressed image (C) due to hemorrhagic degeneration. Note the fetus (white arrowheads).

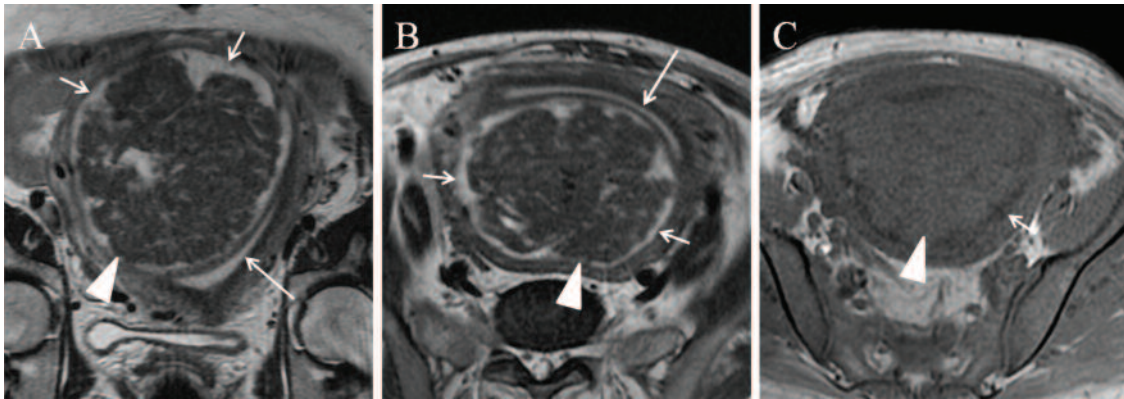


**Figure 8.** Leiomyoma with peripheral edema in a 45 year-old woman. Oblique coronal (A) and oblique axial (B) FSE T2-weighted images reveal a voluminous leiomyoma with low signal intensity (*white arrowheads*) located in the posterior side of the uterine fundus and corpus which displaces forward the endometrial cavity (*long white arrows*). On the outskirts of the lesion can be observed a hyperintense ring (*short white arrows*) due to peripheral edema. (C) On the axial gradient-echo T1-weighted 2D image the leiomyoma (*white arrowhead*) looks isointense compared to the myometrium and the peripheral edema looks hypointense (*short white arrow*).

*Hemorrhage and necrosis* are uncommon histological features that can be observed in leiomyomas; histologically damaged smooth muscle cells are replaced by collagen tissue<sup>3</sup>.

At MR imaging, leiomyomas with necrosis and hemorrhage show inhomogeneous appearance because of the presence of areas with variable signal intensity. In case of ischemic necrosis

areas with hyperintense signal on T2-weighted images and hypointense signal on T1-weighted images may be observed; when hemorrhagic phenomena occur (coagulative-hemorrhagic necrosis) areas with hypointense signal on T2-weighted images and hyperintense signal on T1-weighted images may be observed. After administration of contrast agent necrotic areas don't show contrast enhancement (Figures 9, 10)<sup>1-3</sup>.

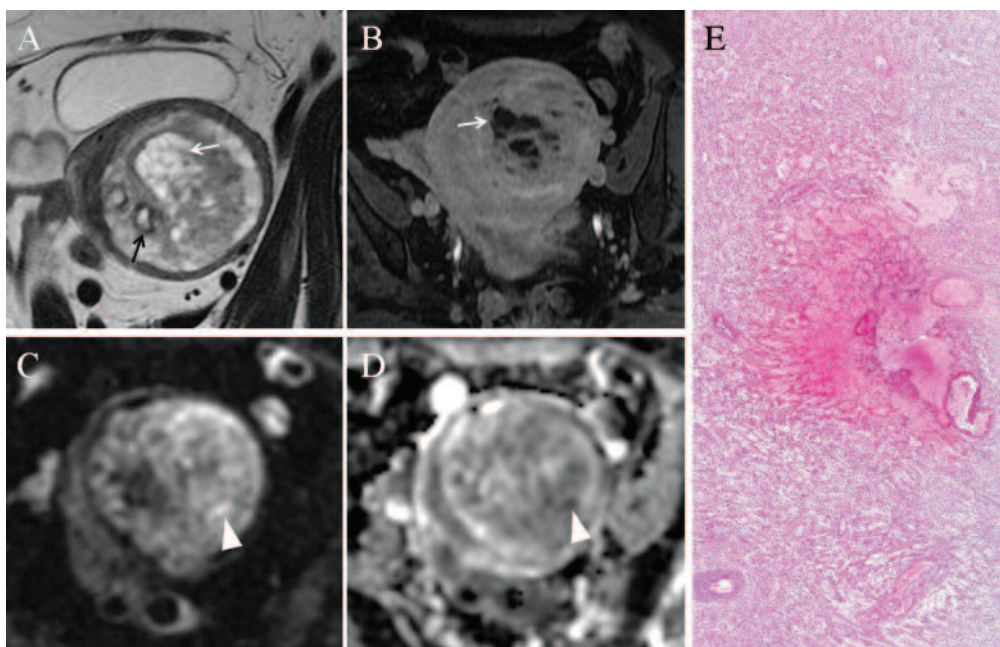


**Figure 9.** Hypercellular leiomyoma with ischemic and hemorrhagic necrosis in a 64 year-old woman. (A) Oblique axial FSE T2-weighted image reveals a leiomyoma with inhomogeneous signal intensity due to the presence of hyperintense areas with fluid content (ischemic necrosis) (*white arrow*) and hypointense areas of hemorrhagic nature (hemorrhagic necrosis) (*black arrow*). (B) Oblique coronal T1-weighted 3D gradient echo LAVA fat-suppressed images after contrast agent administration reveals the presence of hypointense areas with fluid content, without enhancement (ischemic necrosis) (*white arrow*). (C) Axial diffusion-weighted (DW) image ( $b = 800 \text{ s/mm}^2$ ) reveals the presence of hyperintense areas into the lesion (*white arrowheads*), that appear hypointense in the ADC map (*white arrowheads* in D), expression of hypercellularity. (E) Histological examination (H&E 1x). Area of hemorrhagic necrosis.

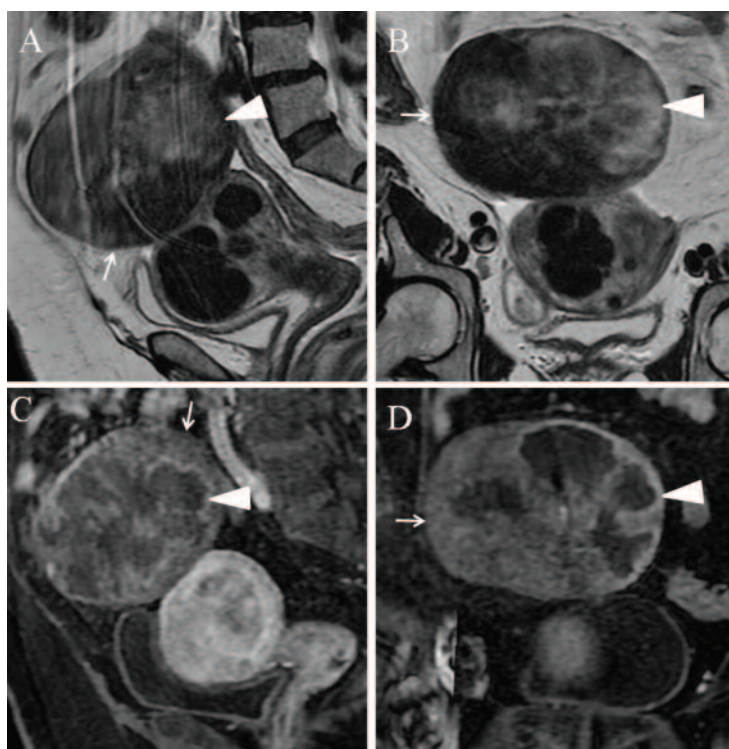


**Figure 10.** Same patient of figure 5. Subserosal pedunculated leiomyoma with ischemic necrosis. Sagittal (A) and oblique coronal (B) FSE T2-weighted images reveal a voluminous subserosal pedunculated leiomyoma of the uterine fundus (white arrows) with inhomogeneous signal intensity due to the presence of hyperintense areas on the posterior and left side (white arrowheads). Sagittal (C) and oblique coronal (D) T1-weighted 3D gradient echo LAVA fat-suppressed images after contrast administration. The mass (white arrows) presents inhomogeneous signal intensity due to the presence of a wide and irregular area without contrast enhancement (white arrowheads). The finding is suggestive of ischemic necrosis.

However it is important to remember that hemorrhage and necrosis occur also in leiomyosarcomas<sup>12</sup>; in these cases, as will be seen below, in the absence of MR features suggestive of malignant transformation (irregular margins) the diagnosis is often exclusively histological<sup>1</sup>.

*Calcifications* occur in about 4% of leiomyomas. They are generally dense and amorphous and can be easily identified at plain abdominal X-ray examination. Rarely may show ring appearance at the periphery of the lesion, as result of a previous hemorrhagic degeneration<sup>3</sup>.

## DIFFERENTIAL DIAGNOSIS

Differential diagnosis of leiomyomas includes adenomyosis, solid adnexal masses, focal contraction of myometrium and leiomyosarcomas of the uterus<sup>1,4</sup>.

### Adenomyosis

At histological examination adenomyosis is characterized by ectopic endometrial glands and stroma inside the myometrium associated with reactive hypertrophy of smooth muscle cells of the surrounding myometrium. Adenomyosis may be focal or diffuse. Clinically may determine dysmenorrhea and menorrhagia, symptoms similar to that of leiomyomas<sup>1,3</sup>.

At MR imaging the diffuse form looks like a thickening of the junctional zone on T2-weighted images (a thickness of the junctional zone superior to 12 mm is highly suggestive of adenomyosis)<sup>13</sup>; hypointense signal of adenomyosis on T2-weighted images is due to the hypertrophy of smooth muscle cells. Small hyperintense foci on T2-weighted images represent endometrial glands; some of these foci may show high signal intensity on T1-weighted images due to hemorrhagic phenomena. In the focal form adenomyosis looks like an area with ill-defined margins into the myometrium with low intensity signal on T2-weighted images, whereas leiomyomas often appear as well defined masses<sup>1,4</sup>. The distinction between adenomyosis and leiomyomas is of clinical importance because leiomyomas may be treated with surgical myomectomy whereas adenomyosis may need hysterectomy<sup>1</sup>.

### Solid adnexal masses

Pedunculated leiomyomas which develop into the broad ligament may enter in differential diagnosis with solid adnexal masses originated by the ovary<sup>1,4</sup>. In the presence of an adnexal mass, on MR imaging, the diagnosis of leiomyoma can be suggested by the demonstration of its continuity with the myometrium even if only for the presence of bridging vessels<sup>14</sup>. The capability of MRI to demonstrate a normal morphology of the ovaries in presence of an enlarged and fibromatous uterus

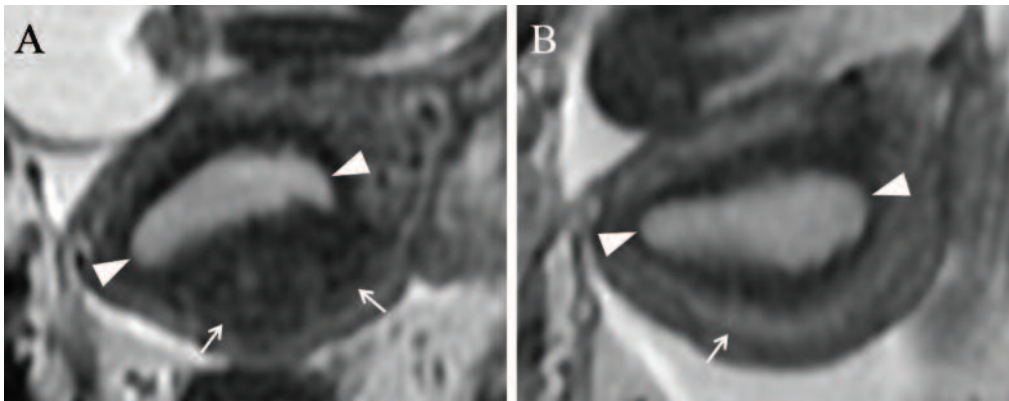


**Figure 11.** Focal myometrium contraction in a 19 year-old woman. (A) Oblique axial FSE T2-weighted image shows a hypointense area (*white arrows*) within the myometrium of the posterior uterine wall. (B) Oblique axial FSE T2-weighted image acquired about 10 minutes later shows homogeneous signal intensity of the myometrium thus excluding the diagnosis of leiomyoma. The finding is suggestive of focal contractions of myometrium. Note the different shape of the endometrial cavity (*white arrowheads* in A and B) due to myometrial contractions.

allows to rule out the diagnosis of adnexal neoplasms. The adnexal neoplasms that may show a signal intensity similar to that of leiomyomas, are ovarian fibromas and Brenner tumor, both characterized by abundant fibroid component. At MR imaging the visualization of ovarian stroma and follicles surrounding an ovarian fibroma or a Brenner tumor allows to establish the ovarian origin of the mass and to exclude the diagnosis of leiomyoma<sup>1,4</sup>. The distinction between an ovarian mass and leiomyoma may be important in pregnant patients as a diagnosis of leiomyoma can exclude the need for surgical treatment<sup>1,4</sup>.

#### ***Focal contraction of myometrium***

At MR imaging focal contractions of myometrium may appear as hypointense areas on T2-weighted images. The transitional nature of these alterations allows to distinguish them from leiomyomas (Figure 11)<sup>15</sup>.

#### ***Leiomyosarcoma of the uterus***

Leiomyosarcomas represent about 30% of uterine sarcomas<sup>16</sup>. Leiomyosarcoma may originate from a pre-existent benign leiomyoma or de novo from the smooth muscle cells of the myometrium. The prevalence of the sarcomatous degeneration of uterine leiomyomas range between 0.1% and 0.8%<sup>17</sup>.

Generally leiomyosarcoma manifests with a significant increase of dimensions of the uterus and is characterized by irregular central areas of hemorrhage and necrosis<sup>4</sup>. At MR imaging, the presence of irregular margins of an uterine leiomyoma may be suggestive of malignant degeneration<sup>1,4</sup>. However the ability of MR to distinguish a degenerated leiomyoma from a leiomyosarcoma hasn't been es-

tablished yet and often the diagnosis of leiomyosarcoma is confirmed by the pathologist after surgical removal of an alleged benign leiomyoma<sup>1</sup>. Histologically leiomyosarcoma is characterized by a rich proliferation of smooth muscle cells, in which several mitosis, nuclear atypia and necrosis are found.

Among other sarcomatous lesions of the uterus the stromal sarcoma (Figure 12) may show very similar MR features to that of leiomyomas; in these cases the diagnosis is exclusively histological.

### **IMAGING PROTOCOL**

The MR imaging protocol we use in our institution to study patients with clinical suspicion or ultrasound finding of uterine leiomyomas is as follows.

MR imaging is performed with a closed-configuration superconducting 1.5-T system (Signa HDxT; GE Healthcare, Milwaukee, Wis) with 57.2 mT/m gradient strength and 120 T/m/s slew rate, by using an eight-channel high-resolution torso coil with array spatial sensitivity technique (ASSET) parallel acquisition.

#### ***MR sequences***

- Localizer sequence in the three spatial planes;
- Axial T2-weighted single-shot fast spin-echo (SSFSE) sequence [time to repetition (TR)/time to echo (TE) range 765/59; flip angle 90°; section thickness 6 mm; interslice gap 0.6 mm; bandwidth 31.25 kHz; field of view (FOV) 38 cm; matrix 320×288; number of averages 0.54; number of images 30; acquisition time 24 s] used as second localizer to identify the longitudinal axis of the uterus in the case of laterally deviated uterus;



**Figure 12.** Stromal sarcoma of the uterus in a 60 year-old woman. (A) Oblique coronal FSE T2-weighted image reveals a homogeneously hypointense lesion (*white arrow*) compared with the myometrium. (B) In oblique coronal T1-weighted 3D gradient echo LAVA fat-suppressed image after contrast administration the lesion presents homogeneous contrast enhancement (*white arrow*). The finding had suggested the diagnosis of leiomyoma. (C) Histological examination (H&E 20x). Low grade endometrial stromal sarcoma: proliferation of small sized, roundish cells which remember the cells of the cytotogen stroma of the uterus; presence of numerous vessels of small caliber surrounded by neoplastic cells.

- Sagittal T2-weighted fast spin-echo (FSE) sequence parallel to the longitudinal axis of the uterus (identified on the previous SSFSE sequence) (TR/TE range 4,675/100; flip angle 90°; section thickness 4 mm; interslice gap 1 mm; bandwidth 41.67 kHz; FOV 32 cm; matrix 320×224; number of averages 4; number of images 26; acquisition time 3 min 49 s);
  - Oblique coronal T2-weighted FSE sequence parallel to the longitudinal axis of the uterus (TR/TE range 4,675/100; flip angle 90°; section thickness 4 mm; interslice gap 1 mm; bandwidth 41.67 kHz; FOV 32 cm; matrix 320×224; number of averages 4; number of images 26; acquisition time 3 min 49 s);
  - Oblique axial T2-weighted FSE sequence perpendicular to the longitudinal axis of the uterus (TR/TE range 4,675/100; flip angle 90°; section thickness 4 mm; interslice gap 1 mm; bandwidth 41.67 kHz; FOV 32 cm; matrix 320×224; number of averages 4; number of images 26; acquisition time 3 min 49 s);
  - Axial DWI SE EPI (TR/TE 3000/74,1; flip angle 90°; section thickness 5 mm; interslice gap 1 mm; bandwidth 250 kHz; field of view 45 cm; matrix 160 × 160; number of averages 16; number of images 14; b-value 0 e 800 s/mm<sup>2</sup>; acquisition time 1 min e 40 s);
  - Sagittal T1-weighted 3D gradient-echo liver acquisition with volume acquisition (LAVA) sequence with fat suppression (TR/TE range 4.4/2.1; flip angle 12°; section thickness 3.4 mm; overlap locations -1.7 mm; bandwidth 62.5 kHz; FOV 40 cm; matrix 320 × 192; number of averages 0.75; number of images 104; acquisition time 22 s).
  - After i.v. administration of 0.1 mmol/kg paramagnetic contrast agent (Dotarem, Guerbet, Roissy, France) at a flow rate of 2 ml/s, followed by 20 ml of saline solution at the same flow rate, the following sequences are acquired:
    - Dynamic sagittal T1-weighted 3D gradient-echo LAVA with fat suppression (TR/TE range 4.4/2.1; flip angle 12°; section thickness 3.4 mm; overlap locations -1.7 mm; bandwidth 62.5 kHz; FOV 40 cm; matrix 320 × 192; number of averages 0.75; number of images 104; acquisition time 22 s) acquired at 60 and 120 s after contrast administration;
    - T1-weighted 3D gradient echo LAVA fat-suppressed sequence, in the coronal oblique (parallel to the longitudinal axis of the uterus), axial oblique (perpendicular to the longitudinal axis of the uterus) and axial planes (TR/TE range 4.4/2.1; flip angle 12°; section thickness 3.4 mm; overlap locations -1.7 mm; bandwidth 62.5 kHz; FOV 40 cm; matrix 320×192; number of averages 0.75; number of images 104; acquisition time 22 s).
- The following optional sequences can be added to the standard ones:
- Sagittal, axial oblique or coronal oblique fat suppressed T2-weighted FSE sequence (TR/TE range 4,675/100; flip angle 90°; section thickness 4 mm; interslice gap 1 mm; bandwidth 41.67 kHz; FOV 32 cm; matrix 320×224; number of averages 4; number of images 24; acquisition time 3 min 49 s);
  - Axial T1-weighted 2D gradient-echo (GRE) sequence in-out (chemical-shift imaging) (TR/TE 180/2,1; flip angle 80°; section thickness 6 mm; interslice gap 0,6 mm; bandwidth 62,5 kHz; field of view 38 cm; matrix 256 × 224 ; number of averages 1; number of images 20; acquisition time 22 s).

MR imaging is performed with the patient lying in the supine position (feet first). T2-weighted FSE sequences are acquired with patient breathing freely, T1-weighted 3D gradient echo LAVA fat-suppressed sequence are acquired in breath hold.

## POTENTIAL ROLE OF DIFFUSION WEIGHTED IMAGING

Diffusion weighted MR imaging (DWI) represents a new perspective of MRI applied to the study of abdominal pathologies. DWI is a technique based on the diffusion motion of water molecules<sup>18</sup>, that displays information about extracellular compartment, tissue cellularity and the integrity of the cellular membranes<sup>19</sup>. In the oncological setting this technique has been applied in the prediction and early detection of response to proton-beam therapy in ocular melanoma<sup>20,21</sup>, in the study of head and neck squamocellular carcinoma<sup>22</sup> and of liver neoplasms<sup>23</sup>. Other applications are represented by the study of inflammatory bowel diseases<sup>24</sup>, the assessment of liver fibrosis<sup>25</sup> and the noninvasive evaluation of transplanted kidney's function<sup>26</sup>.

In our MR protocol we use a DW sequence with b-value of 0 and 800 s/mm<sup>2</sup> that represent the best compromise between signal to noise ratio (SNR) and lesion detection sensitivity on our MR system. In the study of uterine leiomyomas DWI could be of help in identifying hypercellular components of hypercellular leiomyomas or leiomyosarcomas, but its role in the differential diagnosis is still debatable.

Leiomyomas represent one of the main causes of error in the evaluation of myometrial invasion in endometrial carcinoma with MRI<sup>27</sup>. DW sequences could improve the capacity of MRI in staging endometrial cancer because are not influenced by standard pitfalls reported in the literature<sup>28</sup>.

## CONCLUSIONS

Owing to its excellent contrast resolution and multi-planar capabilities MR imaging allows to identify and localize uterine leiomyomas and to distinguish them from other masses of adnexal origin. Characterization of leiomyomas is often possible with MR imaging, but the radiologist should be aware of the pathological features and the radiological findings that characterize the different types of degeneration; however in the presence of widespread phenomena of necrosis and hemorrhage the diagnosis is often histopathological.

Nevertheless, the contribute of MR imaging is irreplaceable to choose the correct therapeutic strategy and in follow-up after therapy.

## CONFLICT OF INTERESTS:

The Authors declare that they have no conflict of interests.

## REFERENCES

- MURASE E, SIEGELMAN ES, OUTWATER EK, PEREZ-JAFFE LA, TURECK RW. Uterine leiomyomas: histopathologic features, MR imaging findings, differential diagnosis, and treatment. *Radiographics* 1999; 19: 1179-1197.
- MAYER DP, SHIPILOV V. Ultrasonography and magnetic resonance imaging of uterine fibroids. *Obstet Gynecol Clin North Am* 1995; 22: 667-725.
- UEDA H, TOGASHI K, KONISHI I, KATAOKA ML, KOYAMA T, FUJIWARA T, KOBAYASHI H, FUJII S, KONISHI J. Unusual appearances of uterine leiomyomas: MR imaging findings and their histopathologic backgrounds. *Radiographics* 1999; 19 Spec No: S131-145.
- DESHMUKH SP, GONSALVES CF, GUGLIELMO FF, MITCHELL DG. Role of MR imaging of uterine leiomyomas before and after embolization. *Radiographics* 2012; 32: E251-281.
- GARCIA CR, TURECK RW. Submucosal leiomyomas and infertility. *Fertil Steril* 1984; 42: 16-19.
- HUTCHINS FL JR. Uterine fibroids. Diagnosis and indications for treatment. *Obstet Gynecol Clin North Am* 1995; 22: 659-665.
- BUTTRAM VC JR, REITER RC. Uterine leiomyomata: etiology, symptomatology, and management. *Fertil Steril* 1981; 36: 433-445.
- DUDIACK CM, TURNER DA, PATEL SK, ARCHIE JT, SILVER B, NORUSIS M. Uterine leiomyomas in the infertile patient: preoperative localization with MR imaging versus US and hysterosalpingography. *Radiology* 1988; 167: 627-630.
- ZAWIN M, MCCARTHY S, SCOTT LM, COMITE F. High-field MRI and US evaluation of the pelvis in women with leiomyomas. *Magn Reson Imaging* 1990; 8: 371-376.
- HAMM B, KUBIK-HUCH RA, FLEIGE B. MR imaging and CT of the female pelvis: radiologic-pathologic correlation. *Eur Radiol* 1999; 9: 3-15.
- MITTL RL JR, YEH IT, KRESSEL HY. High-signal-intensity rim surrounding uterine leiomyomas on MR images: pathologic correlation. *Radiology* 1991; 180: 81-83.
- KEMPSON RL, HENDRICKSON MR. Pure mesenchymal neoplasms of the uterine corpus: selected problems. *Semin Diagn Pathol* 1988; 5: 172-198.
- MARK AS, HRICAK H, HEINRICHS LW, HENDRICKSON MR, WINKLER ML, BACHICA JA, STICKLER JE. Adenomyosis and leiomyoma: differential diagnosis with MR imaging. *Radiology* 1987; 163: 527-529.
- WEINREB JC, BARKOFF ND, MEGIBOW A, DEMOPOULOS R. The value of MR imaging in distinguishing leiomyomas from other solid pelvic masses when sonography is indeterminate. *AJR Am J Roentgenol* 1990; 154: 295-299.
- TOGASHI K, KAWAKAMI S, KIMURA I, ASATO R, TAKAKURA K, MORI T, KONISHI J. Sustained uterine contractions: a cause of hypointense myometrial bulging. *Radiology* 1993; 187: 707-710.
- RHA SE, BYUN JY, JUNG SE, LEE SL, CHO SM, HWANG SS, LEE HG, NAMKOONG SE, LEE JM. CT and MRI of uterine sarcomas and their mimickers. *AJR Am J Roentgenol* 2003; 181: 1369-1374.



17. JANUS CJ, WHITE M, DOTTINO P, BRODMAN M, GOODMAN H. Uterine leiomyosarcoma: magnetic resonance imaging. *Gynecol Oncol* (1989); 32: 79-81.
18. RECHICHI G, GALIMBERTI S, SIGNORELLI M, PEREGO P, VALSECCHI MG, SIRONI S. Myometrial invasion in endometrial cancer: diagnostic performance of diffusion-weighted MR imaging at 1.5-T. *Eur Radiol* 2010; 20: 754-762.
19. LIN G, NG KK, CHANG CJ, WANG JJ, HO KC, YEN TC, WU TI, WANG CC, CHEN YR, HUANG YT, NG SH, JUNG SM, CHANG TC, LAI CH. Myometrial invasion in endometrial cancer: diagnostic accuracy of diffusion-weighted 3.0-T MR imaging—initial experience. *Radiology* 2009; 250: 784-792.
20. FOTI PV, FARINA R, CORONELLA M, PALMUCCI S, MONTANA A, SIGONA A, REIBALDI M, LONGO A, RUSSO A, AVITABILE T, CALTABIANO R, PUZZO L, RAGUSA M, MARIOTTI C, MILONE P, ETTORRE GC. Diffusion-weighted magnetic resonance imaging for predicting and detecting the response of ocular melanoma to proton beam therapy: initial results. *Radiol Med* 2015; 120: 526-535.
21. RUSSO A, MARIOTTI C, LONGO A, FOTI PV, AVITABILE T, UVA MG, FRANCO LM, BONFIGLIO V, MILONE P, ETTORRE GC, RAGUSA M, PURRELLO M, CALTABIANO R, PUZZO L, REIBALDI M. Diffusion-weighted magnetic resonance imaging and ultrasound evaluation of choroidal melanomas after proton-beam therapy. *Radiol Med* 2015; 120: 634-640.
22. PICCOLI M, PALMUCCI S, ROCCASALVA F, TAIBI R, ETTORRE GC. Head and neck squamocellular carcinoma: added role of diffusion weighted imaging. *WCRJ* 2014; 1: e285.
23. ROCCASALVA F, SIVERINO ROA, PICCOLI M, CAPPELLO G, GIUNTA ML, FARINA R, FOTI PV, MILONE P, PALMUCCI S. Liver MRI in oncological patients: what benefits can we get? A practical minireview. *WCRJ* 2014; 1: e397.
24. FOTI PV, FARINA R, CORONELLA M, PALMUCCI S, OGNIBENE N, MILONE P, CONTI BELLOCCHI C, SAMPERI L, INSERRA G, LAGHI A, ETTORRE GC. Crohn's disease of the small bowel: evaluation of ileal inflammation by diffusion-weighted MR imaging and correlation with the Harvey-Bradshaw index. *Radiol Med* 2015; 120: 585-594.
25. PALMUCCI S, CAPPELLO G, ATTINÀ G, FUCCIO SANZÀ G, FOTI PV, ETTORRE GC, MILONE P. Diffusion-weighted MRI for the assessment of liver fibrosis: principles and applications. *Biomed Res Int* 2015; 2015: 874201.
26. PALMUCCI S, MAURO LA, FAILLA G, FOTI PV, MILONE P, SINAGRA N, ZERBO D, VEROUX P, ETTORRE GC, VEROUX M. Magnetic Resonance with diffusion-weighted imaging in the evaluation of transplanted kidneys: updating results in 35 patients. *Transplant Proc* 2012; 44: 1884-1888.
27. FOTI PV, FARINA R, CORONELLA M, RUGGERI C, PALMUCCI S, MONTANA A, MILONE P, ZARBO G, CALTABIANO R, LANZAFAME S, POLITI G, ETTORRE GC. Endometrial carcinoma: MR staging and causes of error. *Radiol Med* 2013; 118: 487-503.
28. BEDDY P, MOYLE P, KATAOKA M, YAMAMOTO AK, JOUBERT I, LOMAS D, CRAWFORD R, SALA E. Evaluation of depth of myometrial invasion and overall staging in endometrial cancer: comparison of diffusion-weighted and dynamic contrast-enhanced MR imaging. *Radiology* 2012; 262: 530-537.